Soil Dynamics and Earthquake Engineering 153 (2022) 107087

Contents lists available at ScienceDirect

Soil Dynamics and Earthquake Engineering

journal homepage: www.elsevier.com/locate/soildyn

Novel seismic design solution for underground structures. Case study of a 2-story 3-bay subway station

Xiangbo Bu [a,*], Alberto Ledesma [b], Francisco López-Almansa [c,1]

[a] Civil and Environmental Eng. Department, Universitat Politècnica de Catalunya·BarcelonaTech (UPC), Barcelona, Spain
[b] Civil and Environmental Eng. Department, Universitat Politècnica de Catalunya·BarcelonaTech (UPC) and CIMNE, Barcelona, Spain
[c] Architecture Technology Department, Universitat Politècnica de Catalunya·BarcelonaTech (UPC), Barcelona, Spain

ARTICLE INFO

Keywords:
Subway underground stations
Sliding-hinged connections
Rubber bearings
Seismic performance
Seismic damage

ABSTRACT

This paper proposes an innovative seismic design approach for shallow rectangular cut-and-cover underground subway or railway stations. The traditional approach is to design rigid frame-like structures by connecting rigidly the main horizontal and vertical structural elements (side walls, top, bottom and intermediate slabs, and central columns); on the contrary, the proposed strategy consists of joining them by means of hinged and sliding connections, in order to obtain structures whose lateral stiffness is almost zero. The objective of this approach is to be able to adapt to the transverse racking motion imposed by the seismic ground motion without significantly increasing the internal forces in the structural members. The aforementioned flexibility of the joints is achieved by interposing rubber bearings between the connected structural elements. As a case study, an existing 2-story 3-bay subway station located in Southwest China is redesigned with the proposed technology; its seismic performance is numerically investigated by performing nonlinear dynamic analyses for a number of horizontal transverse input ground motions (accelerograms) representing the site seismicity. Such inputs are scaled to fit PGAs ranging from 0.1 to 0.6 g. As expected, the results of the time-history analyses reveal that the seismic damage to the structural members is significantly alleviated in the sliding-hinged alternative solution. This conclusion can be understood as a preliminary confirmation of the satisfactory seismic performance of the proposed technology.

1. Introduction

The nowadays rapid development of buried structures, such as tunnels, underground parking lots, subway and railway stations, etc. provides alternatives to the insufficient ground space. Taking subway stations as an example, according to the International Association of Public Transport [1], there were 11,084 stations spreading over 13,903 km of subway operating lines at the end of 2017 in the world, and in the next few years another 1700 km were to be built. However, recent and past investigation reveals that earthquakes can damage underground stations [2–8]; therefore, further research is required on their seismic design.

The traditional seismic design of underground stations is based on providing sufficient stiffness and strength to absorb the strains imposed by the seismic ground motion without excessive damage. This approach is basically correct and leads to safe constructions, but omits that earthquakes are indirect actions (i.e. imposed displacements): designing stiffer structures generates an increase of the soil-structure interaction force, thus providing little benefit (if any). Another smarter strategy is to try to reduce that force, either by lowering the lateral stiffness of the soil (locally) or the station. The first objective is achieved with seismic isolation [9,10], and the second with structural flexibilization measures [9,10]. Both approaches are briefed in the next two paragraphs, respectively.

- **Seismic isolation.** This technology (also known as shock absorption or seismic reduction) consists of surrounding the station with a soft isolation layer that mitigates the soil restraining effect. This layer can be made of various materials such as rubber, foam or other mixing materials [11–13]. Several studies have examined the seismic performance of underground structures with seismic isolation, either through numerical simulation or experiments [14–20].

* Corresponding author.
E-mail address: xiangbo.bu@upc.edu (X. Bu).
[1] Currently Associate Researcher Natural and Anthropogenic Risks Research Center, Univ. Austral de Chile, Valdivia.

https://doi.org/10.1016/j.soildyn.2021.107087
Received 22 April 2021; Received in revised form 25 October 2021; Accepted 19 November 2021
Available online 2 December 2021

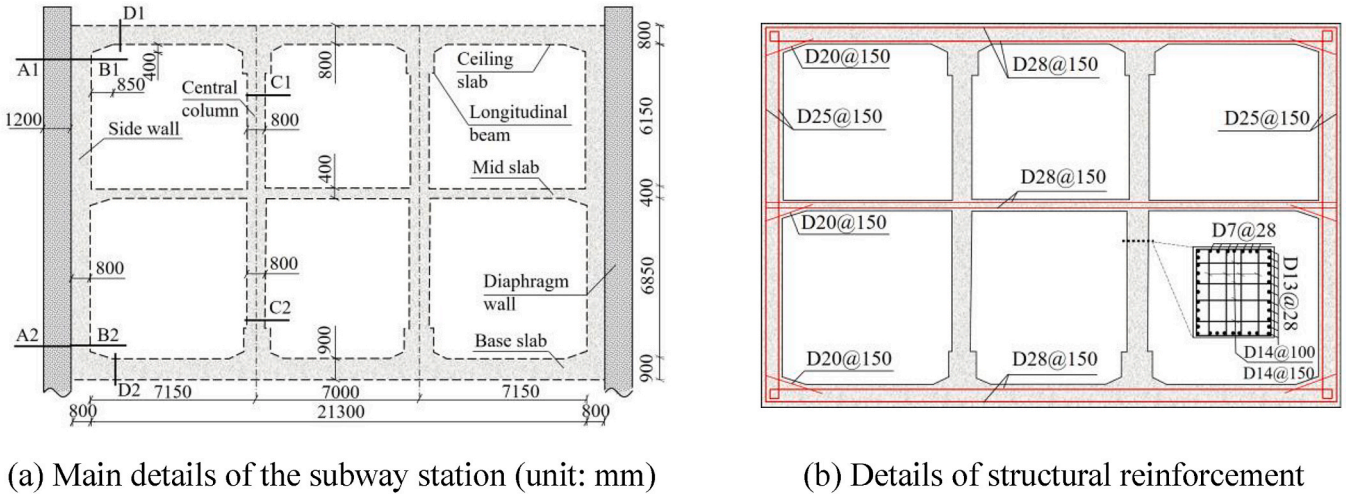

Fig. 1. Original two-story, three-bay subway station.

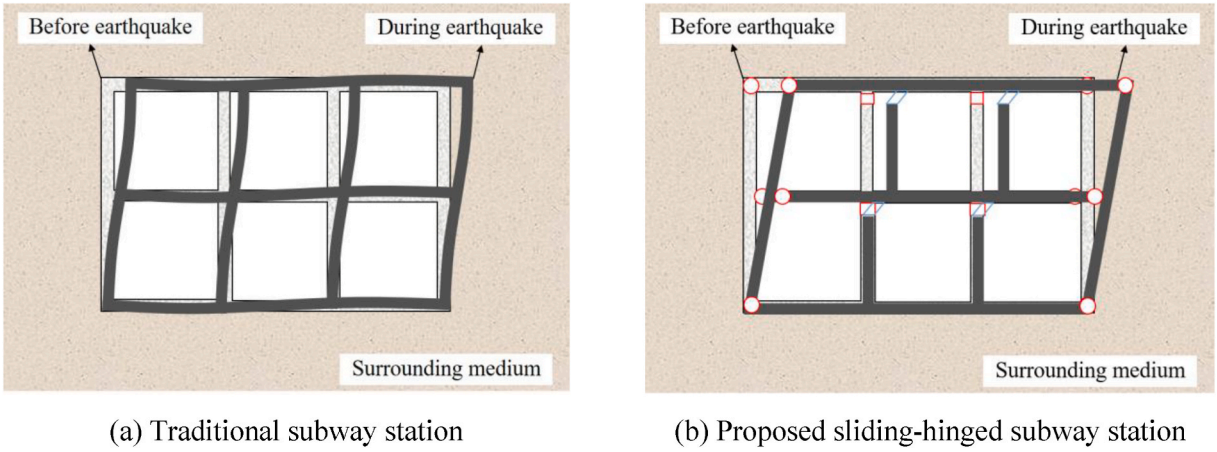

Fig. 2. The working mechanism of different subway stations under earthquake.

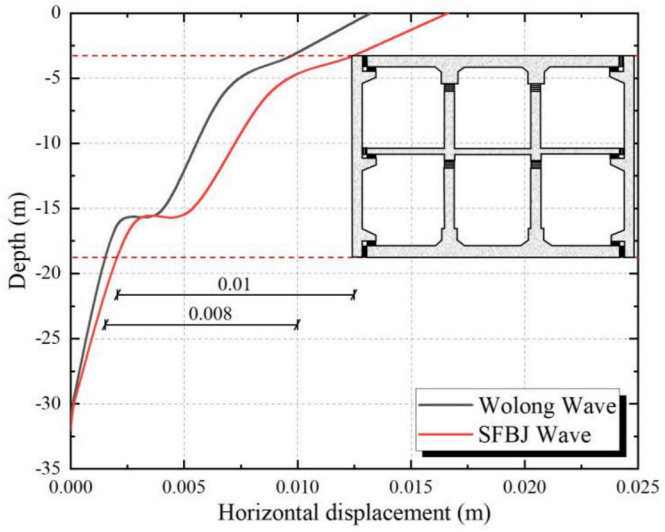

Fig. 3. Free-field racking deformation curve (PGA 0.1 g).

- **Structural flexibilization.** The station lateral stiffness can be decreased by installing flexible joints (sliding bearings or hinges) between the structural members. This approach is mainly utilized in the central columns, as these elements were severely damaged at the well-known Daikai station (Kobe, Japan) [21–25]. Similarly, shear panel dampers [26], lead-rubber bearings [27–29], sliding isolation bearings [10], friction pendulum bearings [30] and natural rubber bearings [31–33], have also been considered. Noticeably, in this strategy, the underground structure is still a rigid frame; although the central columns are protected, damage at slabs and walls can be intensified [33].

This paper participates in the structural flexibilization philosophy, but takes a step forward and proposes to make all the connections flexible, not only those that involve the central columns; the result is a structure whose lateral stiffness is near zero.

To corroborate the feasibility of the proposed solution, the case study of an existing two-story, three-bay subway station located in Chengdu (Southwest China) [34] is analyzed. This station has been chosen mainly because of its complexity, involving several stories and bays. The chosen station had been designed following the classical approach (rigid connections between main structural members); herein, it is redesigned with a novel sliding-hinged solution, where rubber bearings are utilized at the connections between the structural elements. The seismic performance of the proposed solution is analyzed with nonlinear dynamic analyses. The derived conclusions may provide a new perspective for the seismic design of underground structures.

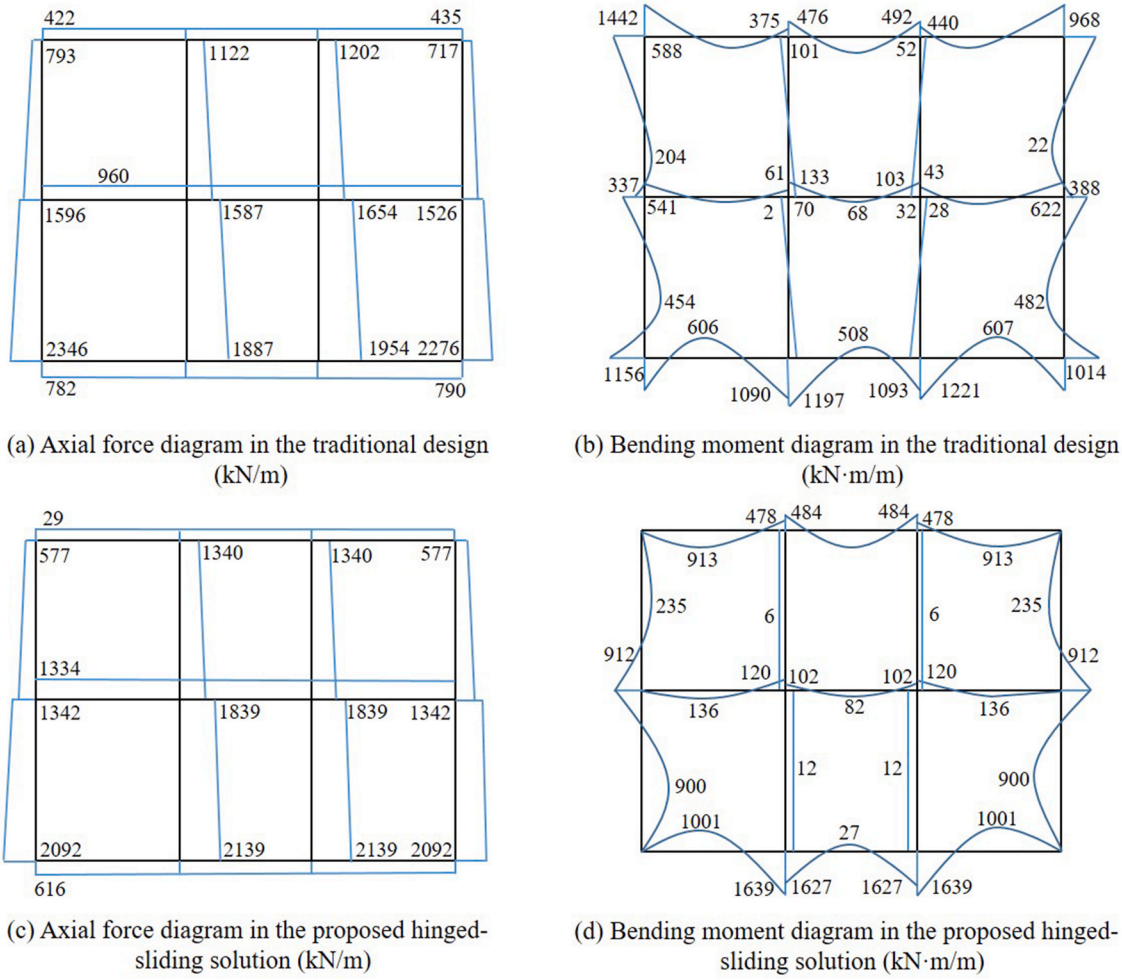

Fig. 4. Internal forces in the subway station.

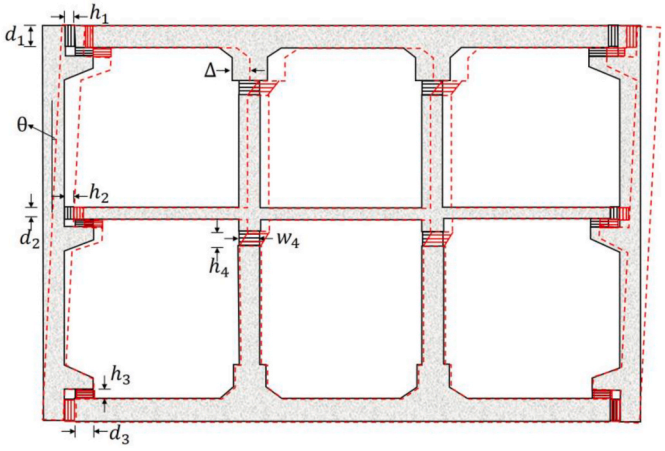

Fig. 5. The detailed sectional dimension of the sliding-hinged subway station.

Table 1
Characteristics of the rubber bearings of the sliding-hinged subway station.

Bearing	Diameter d_i or width w_i (mm)	Height h_i (mm)	Maximum axial force (kN)	Maximum shear displacement (mm)	Maximum rotation angle θ (mrad)
Vertical bearing (1)	300	140	880	±40	21
Vertical bearing (2)	400	140	1880	±54	21
Horizontal bearing (3)	450	140	2390	±54	21
Bearing upon central column (4)	800	170	15,000[a]	±60	24

[a] The longitudinal size of the bearing on the central column is 1 m (as the column).

2. Existing station with traditional structure

As discussed in the Introduction, this paper numerically analyzes the seismic performance of an underground railway station with an innovative structural design based on hinged and sliding connections between its main structural members. The general conditions of this construction (i.e. shape, size and soil type) are based on a real 2-story 3-bay subway station that is located in Chengdu (Southwest China) and has a conventional structural design (rigid connections between its structural elements) [34]; this underground construction is described in this section.

Fig. 1 depicts the main dimensions and structural reinforcement composition of the existing station; Fig. 1 a displays a general transverse

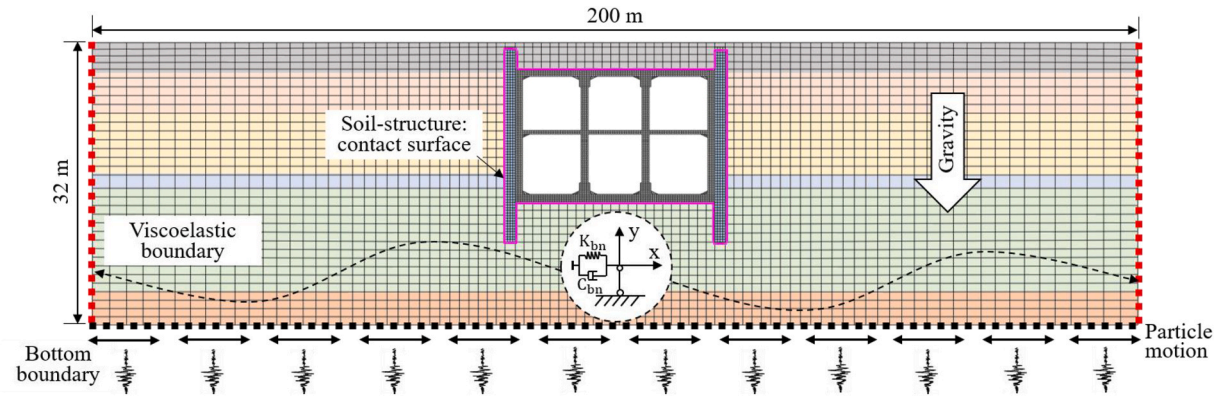

Fig. 6. FE model of the station (traditional and innovative design) and the surrounding soil.

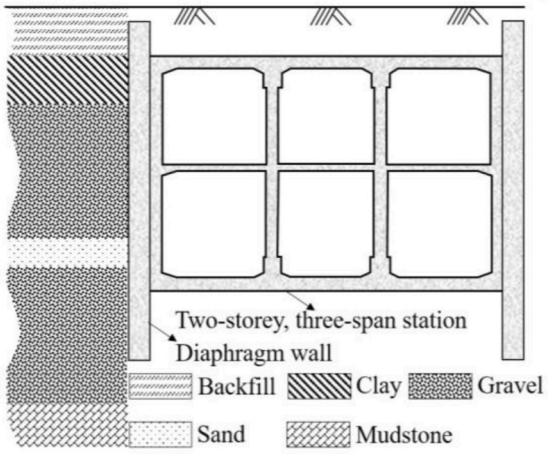

Depth (m)	Density (kg/m^3)	Poisson's ratio	Velocity (m/s)
3	1900	0.33	100
3	2000	0.34	200
9	2100	0.49	300
1.5	1800	0.49	247
12.7	2100	0.49	330
2.8	2300	0.49	400

Fig. 7. Engineering site information of the surrounding medium in the existing station.

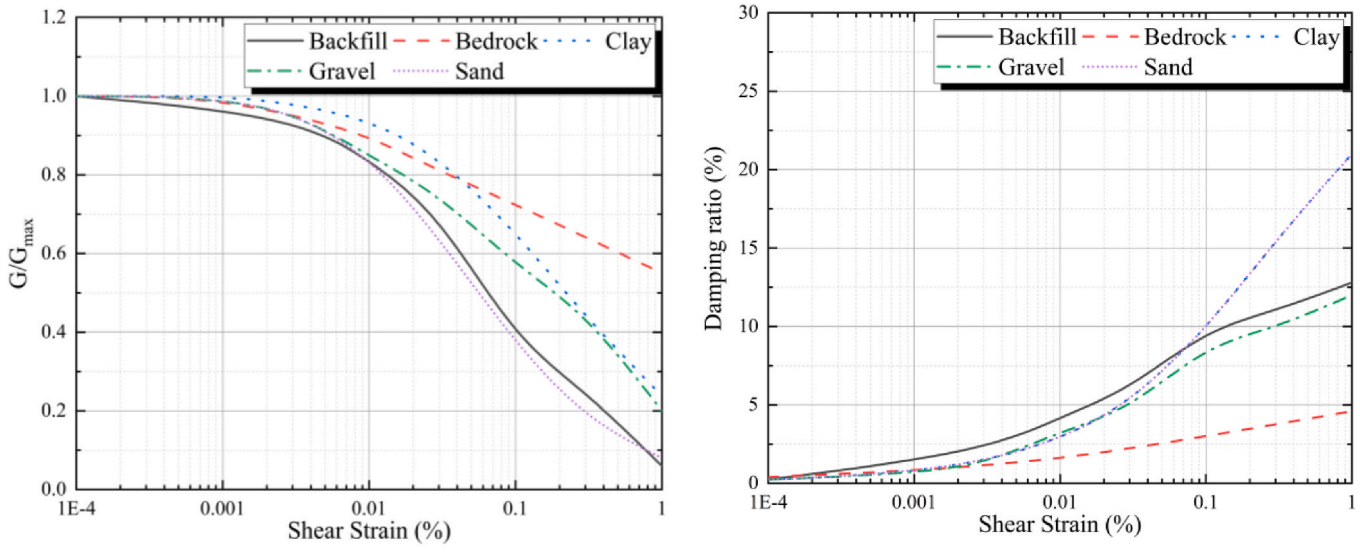

(a) Shear strain– Shear stiffness curves of soil (b) Shear strain– Damping ratio curves of soil

Fig. 8. Site soil information of the subway station [45].

Table 2
Material parameters of concrete in subway station [58].

Elastic modulus (GPa)	Density (kg/m^3)	Poisson's ratio	Dilation angle	Eccentricity	F_{b0}/f_{c0}	K	Viscosity
33.7	2500	0.2	36.3	0.1	1.16	0.667	1e-5

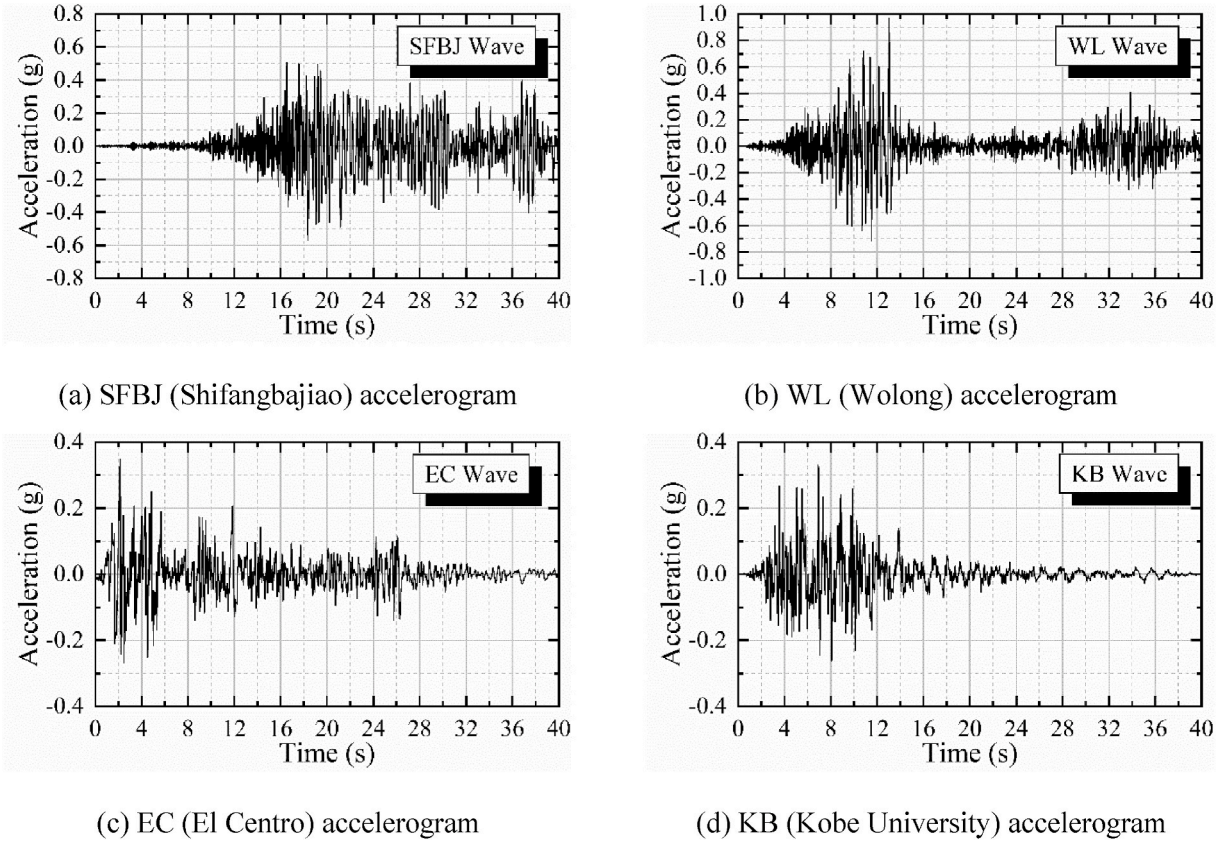

(a) SFBJ (Shifangbajiao) accelerogram (b) WL (Wolong) accelerogram

(c) EC (El Centro) accelerogram (d) KB (Kobe University) accelerogram

Fig. 9. Acceleration time-history records of the four considered earthquake inputs.

section and Fig. 1 b describes the reinforcement. Overall width and height of the station are 22.9 m and 15.1 m; the depth of its top surface is 3 m. The thickness of the ceiling slab, mid slab and bottom slab are 0.8 m, 0.4 m and 0.9 m, respectively; the side wall is 0.8 m thick. Central columns are made of reinforced concrete, with a rectangular cross-section 0.8 and 1 m wide in transverse and longitudinal directions, respectively; columns are spaced 8 m. Fig. 1 a shows that two 1.2 m thick, 22.1 m deep diaphragm walls are located on each side of the station to protect the site during the excavation stage and to provide further additional support; these walls are rigidly connected (tied) to the side walls of the station.

In Fig. 1 a, sections A (diaphragm wall), B (side wall), C (inner column) and D (top and bottom slabs) are selected to later compare the seismic responses of the traditional and proposed sliding-hinged solutions. In Fig. 1 b, D20@150 means that the rebar diameter is 20 mm and their separation is 150 mm.

The peak ground acceleration (PGA) of the subway station is 0.1 g. The soil properties are discussed later in section 4.2.

3. Alternative station with near-zero transverse stiffness

3.1. General description of the alternative structural solution

Fig. 2 displays sketches of traditional (Fig. 2a) and sliding-hinged (Fig. 2b) solutions for the case study station described in section 2. Fig. 2 b shows that the connections between walls and slabs are hinged, while those between interior columns and slabs are sliding; therefore, the lateral stiffness of the station is practically zero.

In Fig. 2 a all the connections are rigid; hence, the structure is statically redundant (hyperstatic), and the imposed seismic lateral racking generates relevant internal forces in the structural members. Conversely, the structure in Fig. 2 b can accommodate racking without significant affectation; noticeably, the central columns do not experience relevant bending.

3.2. Simplified seismic analysis of the alternative structural solution

Traditionally, racking deformation has been considered to dominate the seismic response of rectangular underground structures [35]. However, recent studies have revealed a coupled racking-rocking deformation pattern during transverse ground shaking [36–44]. The demanding racking displacement for the proposed sliding-hinged subway station is estimated by newly proposed R–F relations [43], where F is the flexibility ratio (quotient between the soil and underground structure stiffnesses) and R is the racking coefficient (quotient between the structure and soil relative displacements) [35]:

$$F = \frac{G_s}{S}$$
$$R = \frac{\Delta}{\Delta_{\text{free-field}}} \quad (1)$$

In Eq. (1), G_s is the soil shear modulus, S is the station lateral stiffness; Δ and $\Delta_{\text{free-field}}$ are the racking displacement of the structure

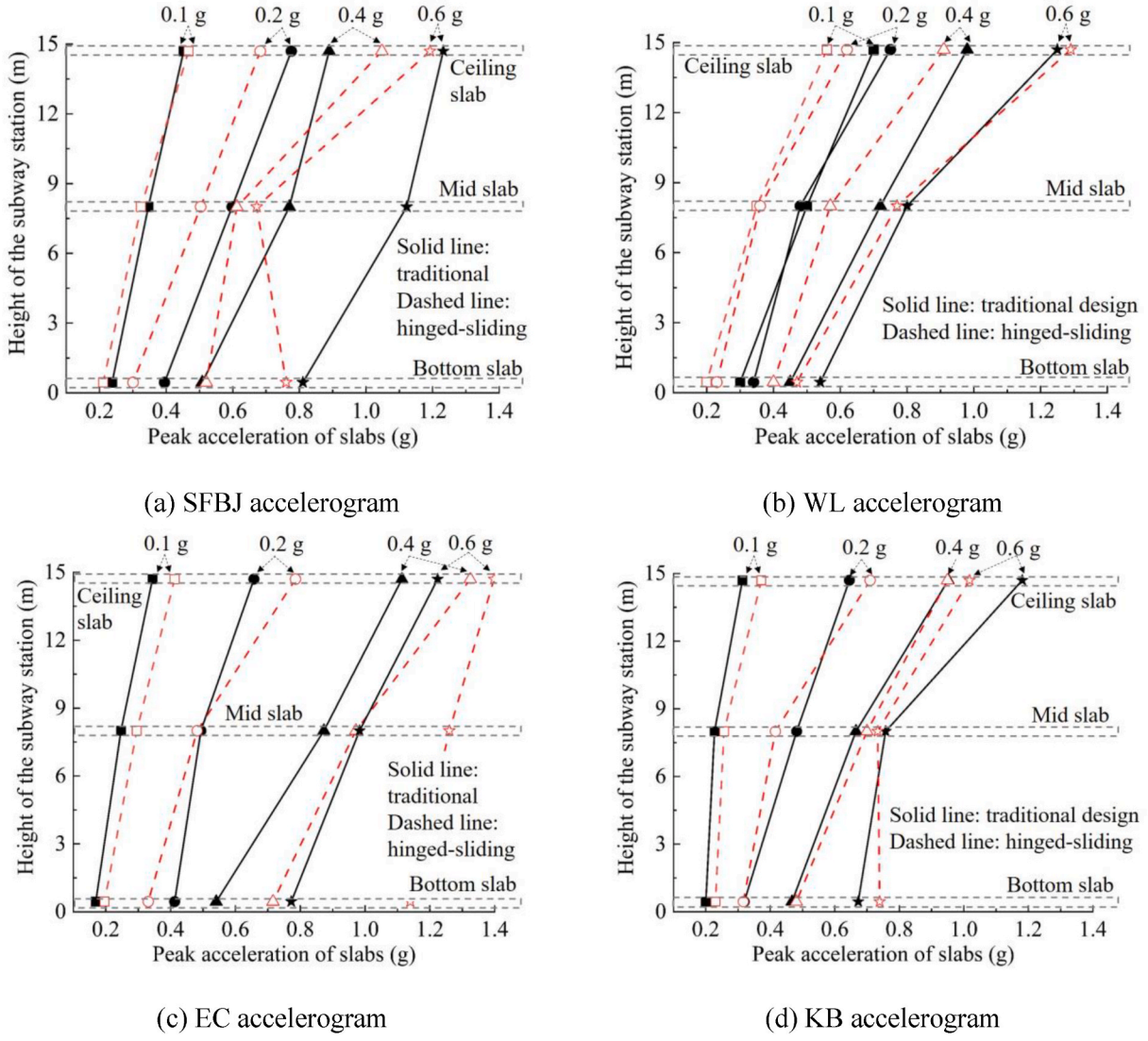

Fig. 10. Peak acceleration of slabs of the subway station under different earthquake inputs.

(including the effect of the rocking rotation) and the free-field one, respectively.

The equivalent-linear program EERA [45] is utilized to calculate the soil lateral displacement. Fig. 3 displays the maximum free-field displacement of the soil for two locally recorded accelerograms corresponding to PGA 0.1 g (section 4.4).

Fig. 3 shows that, for the most demanding input (SFBJ wave), the difference between the maximum free-field soil displacements at the upper and lower level of the structure is 10 mm; then, the demanding racking displacement in the station can be computed as the product of the free-field soil displacement times the racking coefficient due to the near-zero lateral stiffness of the station (that is, with a large value of *F*). The racking coefficient is obtained from a chart in Ref. [43] representing the soil-underground structure interaction; its value is 2.27. Therefore, the station racking displacement is given by 10 mm × 2.27 = 23 mm.

Fig. 4 displays the internal forces (axial force and bending moment) of the subway station with traditional design (Fig. 4 a and Fig. 4b) and the proposed sliding-hinged solution (Fig. 4 c and Fig. 4d), due to the static permanent actions and to the racking imposed displacement simultaneously.

Fig. 4 shows that the axial force and bending moment of traditional and sliding hinge stations are quite similar. Therefore, large changes in the thickness and reinforcement amount of walls, slabs and columns are not expected.

3.3. Preliminary design of the rubber bearings

The required flexibility of the connections (Fig. 2b) is obtained with rubber bearings; this section describes their preliminary design. Their characteristics are obtained from the demanding axial forces and required strains. Regarding this latter issue, Fig. 5 displays a more detailed view of the alternative station than that of Fig. 2 b; this description includes the rubber bearings.

In Fig. 5, d_i and h_i are, respectively, the diameter and height of the bearings connecting the slabs to the side walls; w_4 and h_4 denote, respectively, the width and height of bearings installed upon the central columns; θ and Δ denote the rotation angle and racking displacement of the subway station respectively. As the racking displacement is Δ = 0.023 m, the rotation angle is θ = 23/15,100 = 1.52 mrad.

The geometrical and mechanical parameters (capacity) of the rubber bearings are summarized in Table 1.

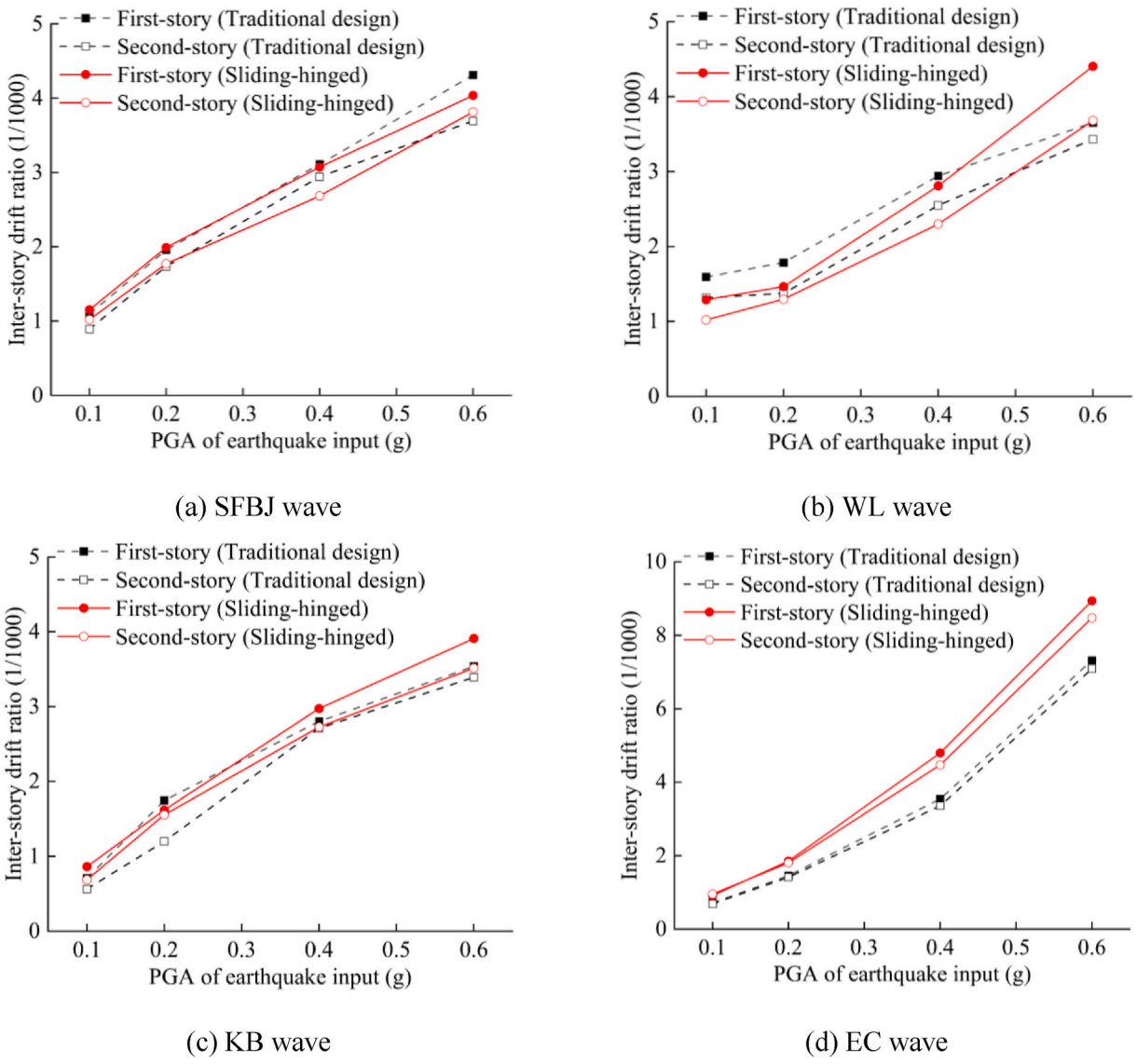

Fig. 11. Maximum inter-story drift ratio of the subway station structure.

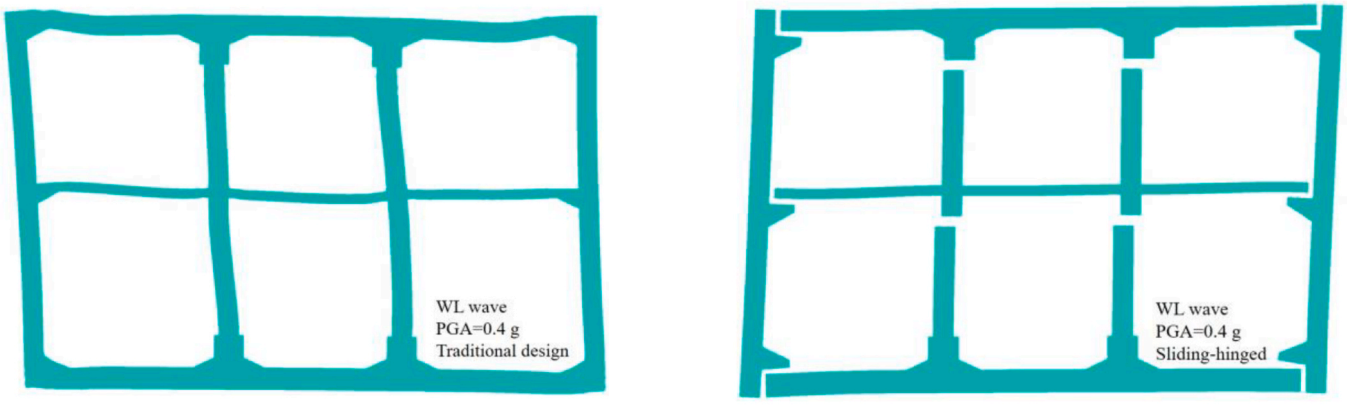

Fig. 12. Deformation the of case study subway station for the input WL scaled to 0.4 g.

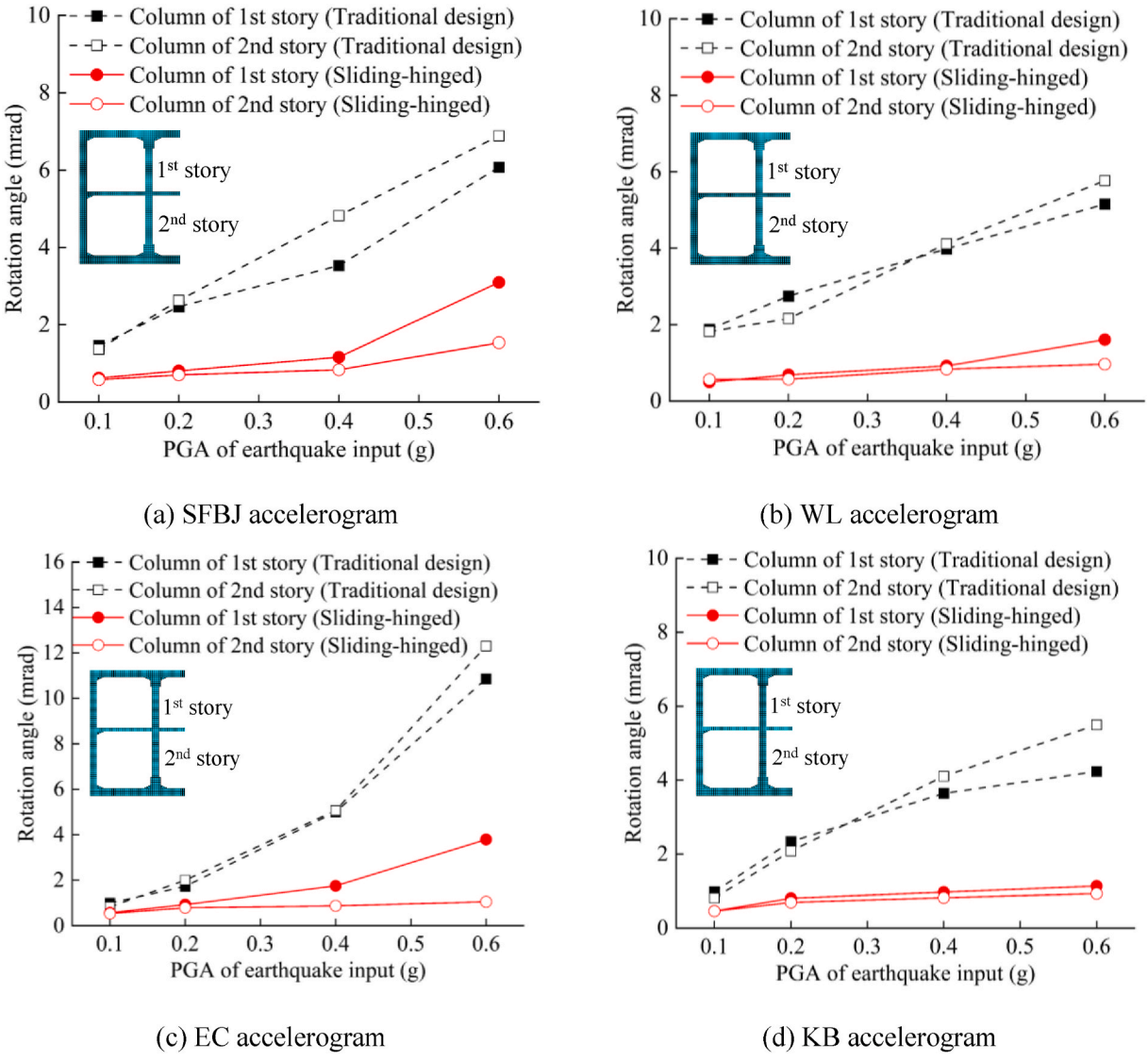

Fig. 13. Rotation angle of the central columns.

4. Finite element analysis of the alternative subway station

4.1. Numerical model of the soil and the structure

As discussed in subsection 3.2, the main dimensions of the structural elements of the existing station, and their reinforcement arrangement (section 2), are maintained in the proposed alternative solution; the soil condition is also taken from the station with traditional design. ABAQUS finite element analysis software [46] is utilized to model soil and structure.

Fig. 6 displays the 2D model of the structure and the surrounding soil; it corresponds to plane strain condition. This model includes both the existing station (traditional design) and the innovative one (sliding-hinged connections).

Fig. 6 shows that the model is 200 m wide; to avoid the influence of the boundary, this value has been selected as approximately 10 times the station width [47]. The analyses are split into static (gravity) and dynamic (seismic) calculations. In the static analyses the lateral boundaries are constrained in horizontal direction and free in the vertical one. In the dynamic analyses the lateral boundaries are modelled as viscoelastic (springs and dashpots) to avoid unrealistic wave bouncing [48–52]; vertical motion is restricted, as only vertical SH wave propagation is considered. In the static analyses the bottom boundary is fixed; in the dynamic analyses its horizontal displacement is released [53,54], as the excitations (horizontal seismic accelerograms) are inputted at the bottom boundary. The stiffness (K_{bn}) and damping (C_{bn}) coefficients of the springs and dashpots are given by Ref. [50]:

$$K_{bn} = A_l \frac{1}{1+A} \frac{\lambda + 2G}{r}$$
$$C_{bn} = A_l B \rho c_p \quad (2)$$

In Eq. (2), A_l is the dominant area of node l; G, ρ are the soil shear modulus and density, respectively; r is the distance between the source of scattering wave and the lateral boundary; $A = 0.8$ and $B = 1.1$; λ is the soil Lamé coefficient; c_p represents the velocity of the compression wave.

The soil and the concrete of the station are discretized with 4-node element CPE4R; the steel reinforcement bars are represented by 2D beam elements. Bond-slip between concrete and steel is not contemplated; as well, in the contact between the sidewalls and the diaphragm walls, no separation is assumed. The element size of the soil-structure interaction model is selected as to range between one eighth and one tenth of the ratio between the shear wave velocity and the cutoff frequency [55]:

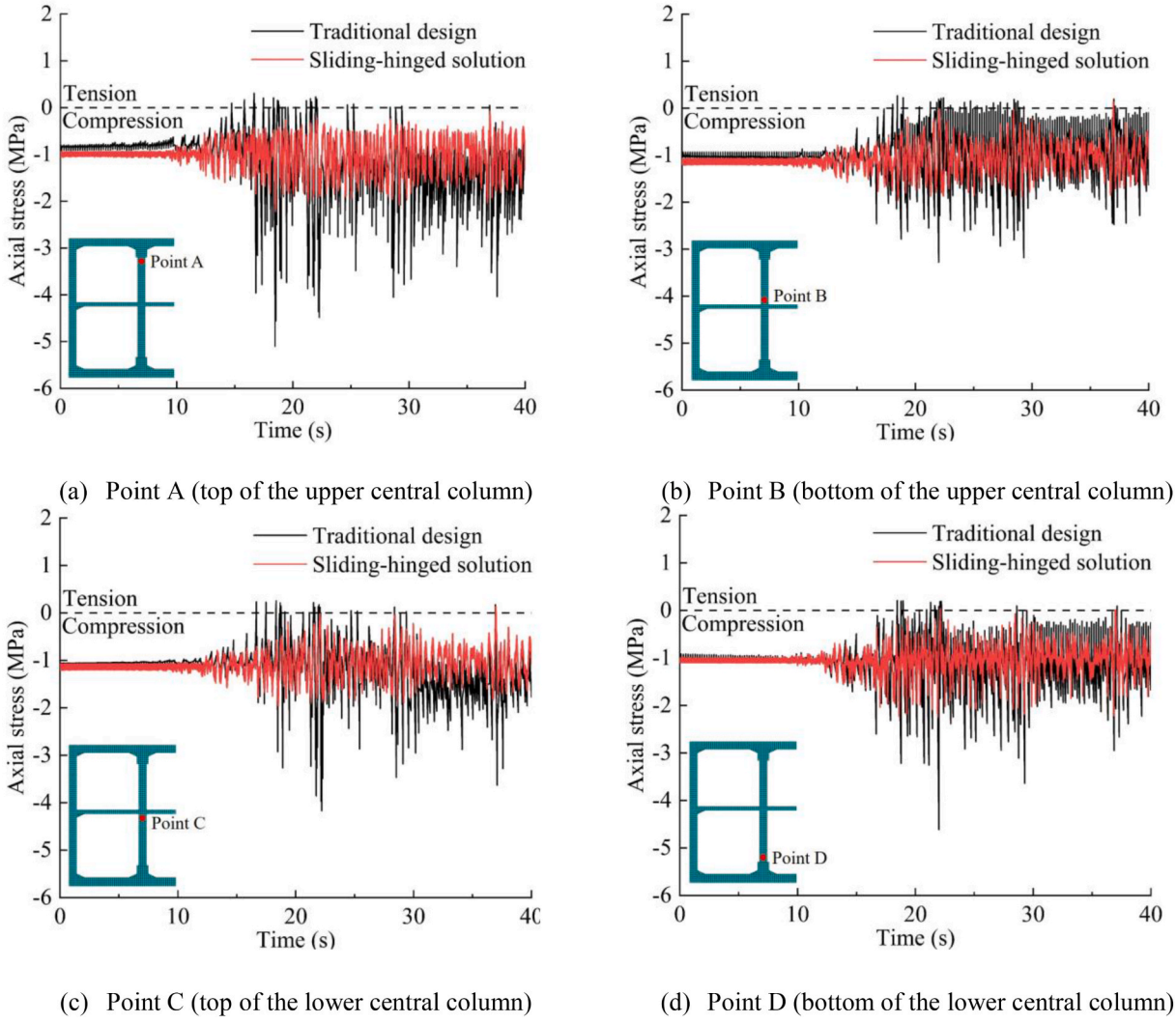

Fig. 14. Stress-time history curves of the central column under SFBJ accelerogram with PGA 0.6 g.

$$\frac{v_s}{10 f_{max}} \le h_{max} \le \frac{v_s}{8 f_{max}} \tag{3}$$

In Eq. (3), v_s is the shear wave velocity, f_{max} is the cutoff frequency and h_{max} is the element size. Thus, the size of the finite elements ranges from 1.4 to 1.8 m.

4.2. Material parameters of the soil and the structure

Fig. 7 displays the main parameters (depth, density, Poisson's ratio and shear wave velocity) of the soil layers.

The soil nonlinear behavior is described with the equivalent simplified method EERA (Equivalent-linear Earthquake site Response Analysis) [45]. Fig. 8 displays the constitutive curves of the G/G_{max} ratio (Fig. 8a) and damping ratio (Fig. 8b) in terms of the shear strain.

The concrete damage plasticity model [56,57] is used; Table 2 presents the major parameters.

In Table 2, F_{b0}/f_{c0} is the ratio between biaxial compressive yield strength and uniaxial compressive yield strength, and K is the ratio between second stress invariants on tensile and compressive meridians. The damage variables evolution is set as in Ref. [58]. The characteristic value of the concrete compressive strength for the slabs, side walls and central columns is 45 MPa, and for the diaphragm wall it is 30 MPa. The elastic modulus and density of the central columns are reduced to convert the spatially distributed columns into plane strain behavior.

Soil damping is described with a mass and stiffness-dependent Rayleigh damping model [59–63]:

$$[C] = \alpha [M] + \beta [K] \tag{4}$$

In Eq. (4), α and β denote Rayleigh damping coefficients, and $[C]$, $[M]$ and $[K]$ are the damping, mass and stiffness matrices, respectively. The Rayleigh damping coefficients are given by:

$$\begin{Bmatrix} \alpha \\ \beta \end{Bmatrix} = \frac{2\zeta_n}{\omega_s + \omega_e} \begin{bmatrix} \omega_s \omega_e \\ 1 \end{bmatrix} \tag{5}$$

In Eq. (5), ζ_n is the equivalent viscous damping obtained from EERA, ω_s is the soil fundamental frequency, and ω_e is the predominant frequency of the earthquake input motion [62,63].

4.3. Simulation of the rubber bearings and the soil-structure contact

As discussed in subsection 3.3, rubber bearings are widely employed because they are capable of providing sufficient vertical bearing and horizontal deformation capacities. This study concentrates on their global behavior as sliding-hinged components, and other issues (influence of ambient temperature, nonlinear behavior etc.) are disregarded.

The contacts between the rubber bearings and the connected elements, and between the station and the surrounding soil (soil-slab and soil-diaphragm wall interaction, respectively) are simulated with the dynamic contact model. In normal direction this model prevents pene-

Fig. 15. Tensile damage nephogram of the station with innovative design. KB wave.

tration under compression while allows separation under tension stress; in the tangential direction the behavior is governed by Coulomb's law of friction:

$$\tau_{critical} = \mu P \tag{6}$$

In Eq. (6), μ is the friction coefficient and P is the normal contact stress. For rubber-concrete interaction μ = 0.025, and for soil-concrete interaction μ = 0.4 [28,33,64,65].

Finally, as discussed in section 2, the connection between the diaphragm walls and the station side walls is assumed to be rigid (neither separation nor sliding) [28,33,66,67].

4.4. Selected seismic input ground motions

Four earthquake records are considered in this study; they are displayed in Fig. 9.

The accelerograms in Fig. 9 are the SFBJ wave (Fig. 9 a, Shifangbajiao station, Wenchuan earthquake 2008, PGA 0.569 g), the WL wave (Fig. 9 b, Wolong station, Wenchuan earthquake 2008, PGA 0.977 g), the EC wave (Fig. 9 c, El Centro, Imperial Valley earthquake 1940, PGA 0.349 g) and the KB wave (Fig. 9 d, Kobe University station, Great Hanshin earthquake 1995, PGA 0.329 g). These ground motions have been downloaded from the PEER-NGA database (http://peer.berkeley.edu/nga/) [68] and the strong-motion seismograph networks (K-NET, KiK-net: https://www.kyoshin.bosai.go.jp/) [69]. The accelerograms in Fig. 9 have been scaled to a maximum acceleration of 0.1 g, 0.2 g, 0.4 g and 0.6 g with a duration time of 40 s.

These four accelerograms have been selected considering that El Centro is widely used in earthquake engineering, and SFBJ, WL and KB have seriously damaged underground structures [28,33,70].

5. Numerical results for the alternative subway station

5.1. Acceleration response

Fig. 10 displays, for each of the four seismic waves (accelerograms) in Fig. 9 scaled to 0.1 g, 0.2 g, 0.4 g and 0.6 g, the maximum lateral acceleration of each slab corresponding to traditional rigid and sliding-hinged connection between the structural components.

Fig. 10 shows that the accelerations in the traditional and innovation design solutions are rather similar; therefore, the same level of damage to acceleration-sensitive nonstructural components is to be expected. This trend is credible, as the seismic effect is basically an imposed displacement, and the seismic response is not highly sensitive to its own stiffness.

5.2. Lateral displacement response

Fig. 11 displays, for each of the four accelerograms in Fig. 9 scaled to 0.1 g, 0.2 g, 0.4 g and 0.6 g, the maximum lateral inter-story drift ratio corresponding to the traditional and innovative design solutions.

Fig. 11 shows that the drifts in the traditional and innovative design solutions are rather similar; therefore, the same level of damage to drift-sensitive nonstructural components is to be expected. As in Fig. 10, this trend is credible, as the seismic action is basically a displacement-controlled action, almost irrespective of the structure itself.

To better explain the influence of the sliding-hinged connections on the seismic behavior of the station, its maximum deformation is

Fig. 16. Compression damage nephogram of the station with innovative design. KB wave.

represented in Fig. 12 taking the WL wave as an example.

Fig. 12 corroborates, in a quantified way, the qualitative trends shown in Figs. 2 and 5. However, Fig. 12 b shows that the deformation of the brackets is significant; hence, they should be given sufficient attention in future research.

5.3. Seismic performance of the central columns

As outlined in section 1, it is widely accepted that central columns constitute the key issue for the seismic performance of underground stations [2,21,22,24], as learned from the collapse of the Daikai station by the Great Hanshin earthquake (January 17, 1995, $M_w = 6.9$). In this section, the seismic performance of the central columns of the case study station is investigated.

Fig. 13 displays, for each of the four accelerograms in Fig. 9 scaled to 0.1 g, 0.2 g, 0.4 g and 0.6 g, the maximum global rotation angle of the central columns. Results in Fig. 13 correspond to the traditional and innovative design solutions.

Fig. 13 corroborates that the rotation angle of the central columns is significantly smaller in the innovative design solution than in the traditional one.

For further clarity, Fig. 14 displays, for the SFBJ wave scaled to PGA 0.6 g, the time histories of the maximum vertical axial stress of the inner columns. Plots in Fig. 14 a, Fig. 14 b, Fig. 14 c and Fig. 14 d correspond to points A, B, C and D, respectively.

Fig. 14 confirms the trends shown by Fig. 13. Noticeably, tension of the central columns is almost totally eliminated in the proposed sliding-hinged solution; this improvement is particularly significant, given that such elements have been the most seriously damaged ones.

5.4. Damage indices

As discussed in subsection 4.2, the nonlinear concrete behavior is simulated with a concrete damage plasticity model; in that model, compressive and tensile damage indices (DAMAGEC and DAMAGET, respectively) range between 0 (no damage) and 1 (entire damage). Fig. 15 and Fig. 16 display, for the KB accelerogram scaled to 0.1 g, 0.2 g, 0.4 g and 0.6 g, color maps of the tensile and compressive damage indices, respectively.

Fig. 15 shows that unsurprisingly, the higher the PGA, the more important the damage. For the traditional design solution, as anticipated [28,29,33,70], the most severe tensile cracking damage occurs at the connection between side walls and slabs, in the end sections of the central columns and mid slabs, and in the sections of the diaphragm walls that adjacent to slabs. In the innovative solution, the cracking damage is dramatically reduced, being totally absent in the central columns; as seen in Fig. 12, it is mainly concentrated in the brackets.

Fig. 16 shows that the compressive crushing damage is significantly lower than the tensile one, being virtually non-existent in the sliding-hinged solution. In fact, only slight crushing damage is observed in the central columns of the traditional solution for PGA 0.6 g.

For deeper information, Fig. 17 displays, for the KB accelerogram, comparisons between the tensile damage indices in characteristic points of the traditional and innovative design solutions.

Fig. 17 shows that the damage in the sliding-hinged solution is significantly smaller, particularly in the central columns and slabs.

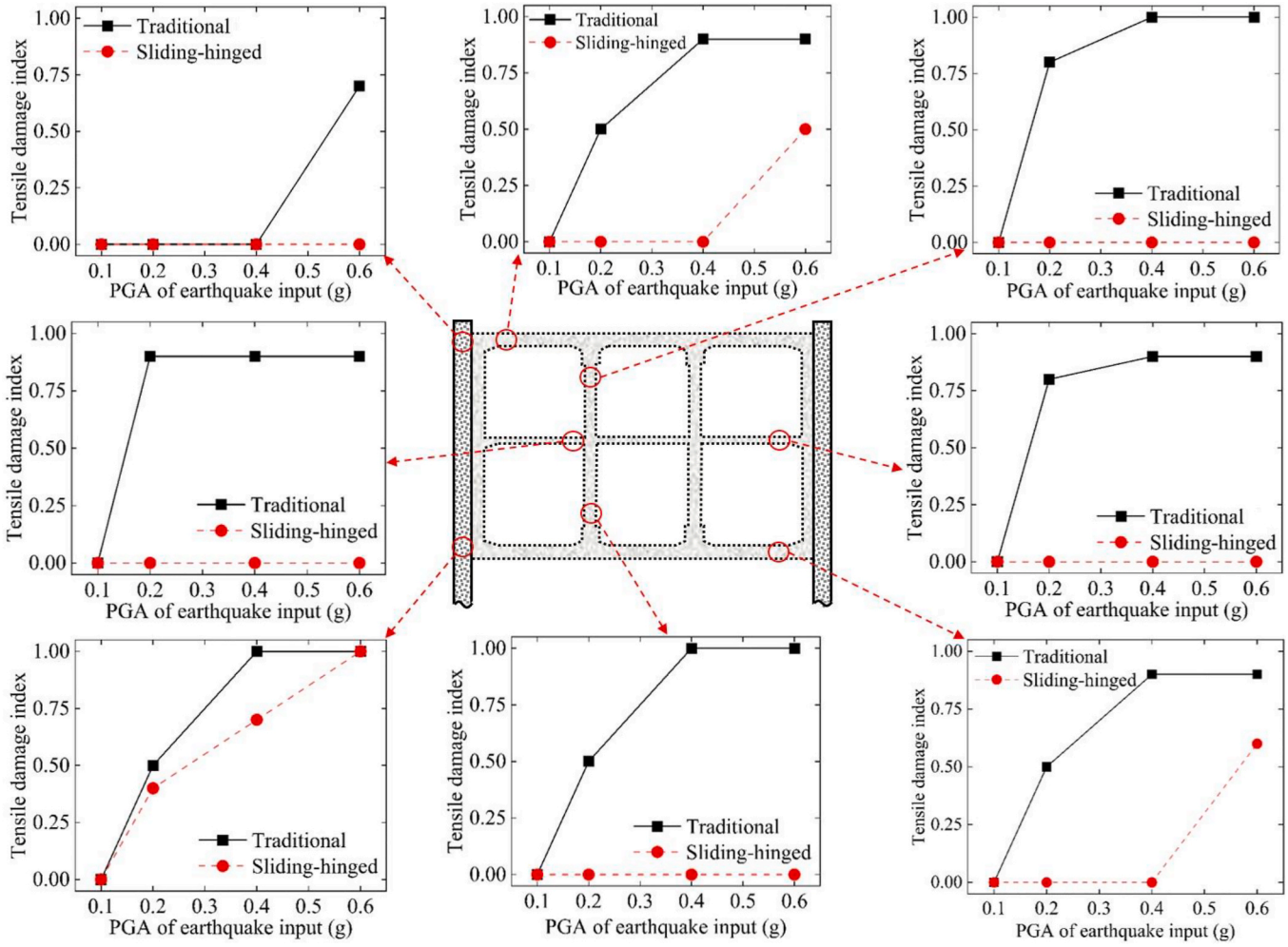

Fig. 17. Tensile damage index of the station. KB wave.

5.5. Comparison between the internal forces of the traditional and innovative stations

Aiming to corroborate the remarks from subsection 5.4, a particular comparison between the internal forces of the members of the traditional and innovative design solutions is presented herein. In this sense, Fig. 18 presents, under the KB seismic wave scaled to 0.1 g, 0.2 g, 0.4 g and 0.6 g, the maximum axial and shear forces and the bending moment in the sections indicated in Fig. 1 a.

Fig. 18 shows that the internal forces in the diaphragm walls (sections A1 and A2) are rather similar in the traditional and innovative stations. In the side walls (sections B1 and B2) the internal forces in the sliding-hinged solution are appreciably smaller. Regarding the interior columns (sections C1 and C2) the reduction is even higher. Finally, the lessening in the ceiling and floor slabs (sections D1 and D2) is also relevant.

6. Conclusions

This paper proposes a new alternative seismic design solution for rectangular cut-and-cover underground stations; it consists of replacing the traditional rigid connections between the structural elements with hinged and sliding joints, as to obtain near-zero lateral stiffness. The required flexibility of the joints is achieved through the use of rubber bearings. The ensuing structures are expected to be able to accommodate the imposed seismic racking without relevant strains in the structure. As a case study, an existing 2-story 3-bay subway station located in Southwest China is redesigned with the proposed technology; its seismic performance is investigated numerically by time-history analyses for a set of input seismic accelerograms. These inputs are scaled to fit PGAs ranging from 0.1 to 0.6 g.

The main output of this study is that the damage to the structural elements is considerably lessened in the sliding-hinged alternative solution; this trend is particularly intense for not only central columns but also structural connections. On the other hand, the acceleration and drift do not alter much; therefore, no higher damage to the acceleration and drift-sensitive nonstructural components is to be expected in the proposed alternative solution. These conclusions hold for all the considered levels of PGA. The remarks obtained can be read as a preliminary validation of the proposed seismic design approach.

Further research (currently under development) includes consideration of other representative case studies, performing parametrical studies to corroborate the general validity of the proposed solution, and deep analysis of the construction issues (e.g. waterproofing system).

Author statement

Xiangbo Bu: Calculations, Graphical Information, Visualization, Software, Writing- Original draft preparation. Alberto Ledesma: Reviewing, Soil-Related Issues, Writing-Reviewing and Editing. Francisco López-Almansa: Conceptualization, Methodology, Seismic-Related Issues, Writing-Reviewing and Editing.

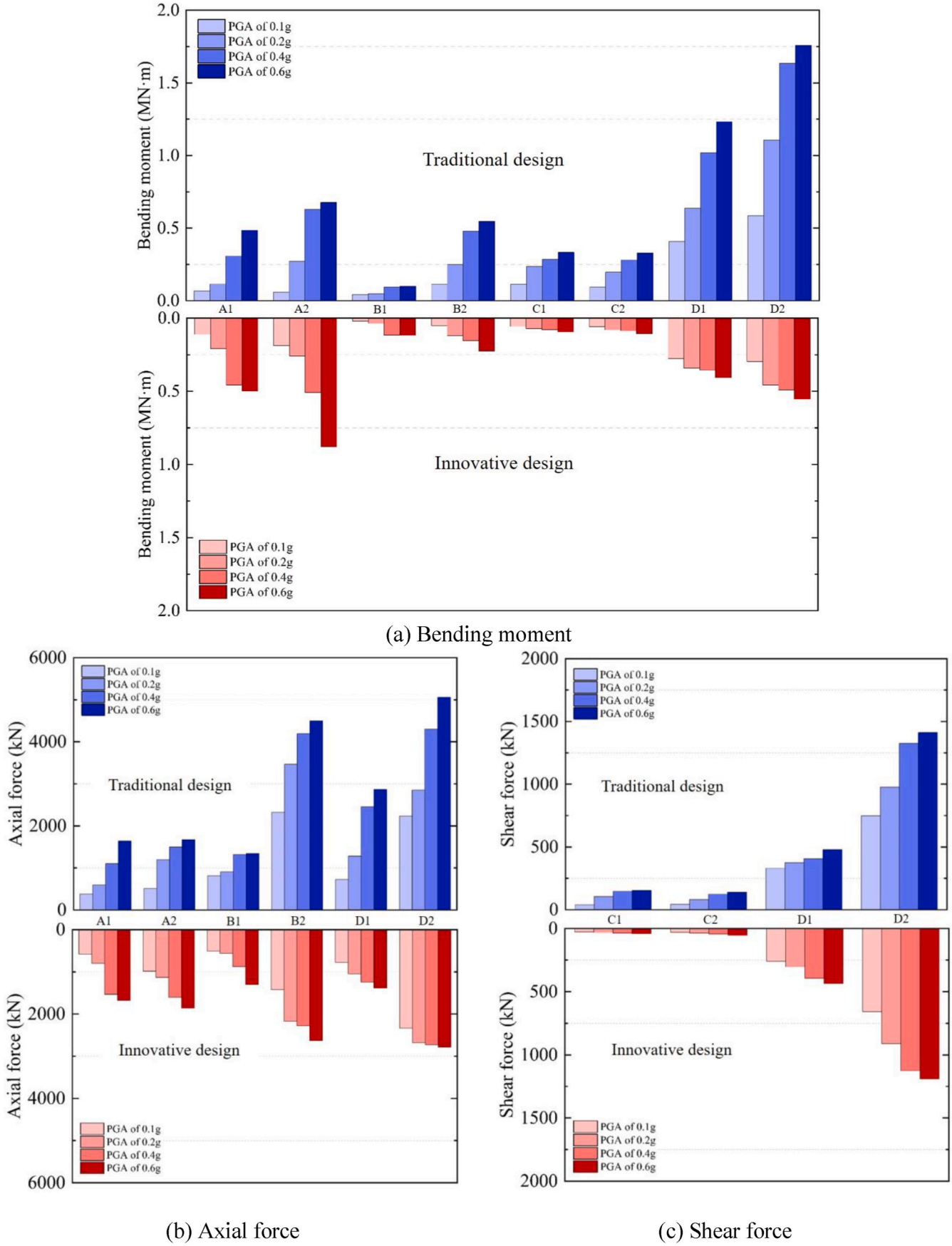

Fig. 18. Maximum internal forces under different ground motion intensities. KB wave.

Declaration of competing interest

The authors declare that they have no known competing financial interests or personal relationships that could have appeared to influence the work reported in this paper.

Acknowledgements

This work has received support from the Chinese Government Scholarship (CSC No. 201906560013) with UPC - Barcelona Tech - CSC joint project, which is gratefully acknowledged.

References

[1] International Association of Public Transport (UITP). World Metro Figures 2018. International Association of Public Transport; 2018. https://www.uitp.org/publications/world-metro-figures/.
[2] Iida H, Hiroto T, Yoshida N, Iwafuji M. Damage to Daikai subway station. Special Soils Found 1996;36:283–300. https://doi.org/10.3208/sandf.36.Special_283.
[3] Hashash YM, Hook JJ, Schmidt B, John I, Yao C. Seismic design and analysis of underground structures. Tunn Undergr Space Technol 2001;16(4):247–93. https://doi.org/10.1016/S0886-7798(01)00051-7.
[4] Wang WL, Wang TT, Su JJ, Lin CH, Seng CR, Huang TH. Assessment of damage in mountain tunnels due to the Taiwan Chi-Chi earthquake. Tunn Undergr Space Technol 2001;16(3):133–50. https://doi.org/10.1016/S0886-7798(01)00047-5.
[5] Shen Y, Gao B, Yang X, Tao S. Seismic damage mechanism and dynamic deformation characteristic analysis of mountain tunnel after Wenchuan earthquake. Eng Geol 2014;180(8):85–98. https://doi.org/10.1016/j.enggeo.2014.07.017.
[6] Yu H, Chen J, Bobet A, Yuan Y. Damage observation and assessment of the Longxi tunnel during the Wenchuan earthquake. Tunn Undergr Space Technol 2016;54:102–16. https://doi.org/10.1016/j.tust.2016.02.008.
[7] Zhang X, Jiang Y, Maegawa K. Mountain tunnel under earthquake force: a review of possible causes of damages and restoration methods. J Rock Mech Geotech 2020;12(2):414–26. https://doi.org/10.1016/j.jrmge.2019.11.002.
[8] Han J, El Naggar MH, Zhao M, Zhong Z, Hou B, Xiuli DU. Longitudinal response of buried pipeline under non-uniform seismic excitation from multi-point shaking table tests. Soil Dynam Earthq Eng 2021;140:106440. https://doi.org/10.1016/j.soildyn.2020.106440.
[9] Wei QH, Sun HF. Status of seismic isolation research on underground structures. Adv Mater Res 2012;594:1611–5. https://doi.org/10.4028/www.scientific.net/AMR.594-597.1611.
[10] Ma C, Lu D, Du X. Seismic performance upgrading for underground structures by introducing sliding isolation bearings. Tunn Undergr Space Technol 2018;74:1–9. https://doi.org/10.1016/j.tust.2018.01.007.
[11] Suzuki T, Tanaka T. Research and development on the seismic isolation system applied to urban tunnels (part-1: development of seismic isolation materials and construction methods). In: Proceedings of the 7th US-Japan Workshop on Earthquake Disaster Prevention for Lifeline Systems. Washington: Seattle; 1997. p. 447–59. https://rosap.ntl.bts.gov/view/dot/42182/dot_42182_DS1.pdf#page=473.
[12] Kim DS, Konagai K. Seismic isolation effect of a tunnel covered with coating material. Tunn Undergr Space Technol 2000;15:437–43. https://doi.org/10.1016/S0886-7798(01)00012-8.
[13] Kim DS, Konagai K. Key parameters governing the performance of soft tunnel coating for seismic isolation. Earthq Eng Struct Dynam 2001;30:1333–43. https://doi-org.recursos.biblioteca.upc.edu/10.1002/eqe.65.
[14] Chen ZY, Shen H. Dynamic centrifuge tests on isolation mechanism of tunnels subjected to seismic shaking. Tunn Undergr Space Technol 2014;42:67–77. https://doi.org/10.1016/j.tust.2014.02.005.
[15] Chen Z, Liang S, Shen H, He C. Dynamic centrifuge tests on effects of isolation layer and cross-section dimensions on shield tunnels. Soil Dynam Earthq Eng 2018;109:173–87. https://doi.org/10.1016/j.soildyn.2018.03.002.
[16] Zhao W, Chen W, Yang D. Interaction between strengthening and isolation layers for tunnels in rock subjected to SH waves. Tunn Undergr Space Technol 2018;79:121–33. https://doi.org/10.1016/j.tust.2018.05.012.
[17] Roy N, Bharti SD, Kumar A. Seismic isolation of tunnels in blocky rock mass using expanded polystyrene (EPS) Geofoam. Innovative Infrastructure Solution 2019;4(1):1–7. https://doi.org/10.1007/s41062-019-0225-0.
[18] Fan K, Shen Y, Wang S, Gao B, Zheng Q, Yan G. Dynamic response of composite lining tunnel with buffer layer: an analytical and experimental investigation. Math Probl Eng 2020;2020:1–17. https://doi.org/10.1155/2020/5453138. 5453138.
[19] Xin CL, Wang ZZ, Yu J. The evaluation on shock absorption performance of buffer layer around the cross section of tunnel lining. Soil Dynam Earthq Eng 2020;131:106032. https://doi.org/10.1016/j.soildyn.2020.106032.
[20] Jiang X, Yu L, Yang H, Zhou W. Shaking table test study of low-buried and unsymmetrical pressure tunnels with rubber shock absorber layer. Geotech Geol Eng 2021;39(1):171–83. https://doi.org/10.1007/s10706-020-01484-2.
[21] An X, Shawky AA, Maekawa K. The collapse mechanism of a subway station during the Great Hanshin earthquake. Cement Concr Compos 1997;19(3):241–57. https://doi.org/10.1016/S0958-9465(97)00014-0.
[22] Huo H, Bobet A, Fernandez G, Ramirez J. Load transfer mechanisms between underground structure and surrounding ground: evaluation of the failure of the Daikai Station. J Geotech Geoenviron Eng 2005;131(12):1522–33. https://doi.org/10.1061/(ASCE)1090-0241(2005)131:12(1522).
[23] Zhuang HY, Cheng S, Chen GX. Numerical simulation and analysis of earthquake damages of Dakai metro station caused by Kobe earthquake. Rock Soil Mechanics Wuhan 2008;29(1):245. https://doi.org/10.16285/j.rsm.2008.01.048.
[24] Ma C, Lu DC, Du XL, Qi CZ, Zhang XY. Structural components functionalities and failure mechanism of rectangular underground structures during earthquakes. Soil Dynam Earthq Eng 2019;119:265–80. https://doi.org/10.1016/j.soildyn.2019.01.017.
[25] Mikami A, Konagai K, Sawada T. Stiffness design of isolation rubber for center columns of tunnel. 2001 Dob Gakkai Ronbunshu 2001;(682):415–20. https://www.jstage.jst.go.jp/article/jscej1984/2001/682/2001_682_415/_pdf.
[26] Chen ZY, Chen W, Bian GQ. Seismic performance upgrading for underground structures by introducing shear panel dampers. Adv Struct Eng 2014;17:1343–57. https://doi.org/10.1260/1369-4332.17.9.1343.
[27] Chen ZY, Zhao H, Lou ML. Seismic performance and optimal design of framed underground structures with lead-rubber bearings. Struct Eng Mech 2016;58:259–76. https://doi.org/10.12989/sem.2016.58.2.259.
[28] Jing Y, Haiyang Z, Wei W, Zhenghua Z, Guoxing C. Seismic performance and effective isolation of a large multilayered underground subway station. Soil Dynam Earthq Eng 2021;142:106560. https://doi.org/10.1016/j.soildyn.2020.106560.
[29] He Z, Chen Q. Upgrading the seismic performance of underground structures by introducing lead-filled steel tube dampers. Tunn Undergr Space Technol 2021;108:103727.
[30] Xu Z, Du X, Xu C, Han R. Numerical analyses of seismic performance of underground and aboveground structures with friction pendulum bearings. Soil Dynam Earthq Eng 2020;130:105967. https://doi.org/10.1016/j.soildyn.2019.105967.
[31] Liu Z, Chen Z, Liang S, Li C. Isolation mechanism of a subway station structure with flexible devices at column ends obtained in shaking-table tests. Tunn Undergr Space Technol 2020;98:103328. https://doi.org/10.1016/j.tust.2020.103328.
[32] Zheng Y, Yue C. Shaking table test study on the functionality of rubber isolation bearing used in underground structure subjected to earthquakes. Tunn Undergr Space Technol 2020;98:103153. https://doi.org/10.1016/j.tust.2019.103153.
[33] Zhuang H, Zhao C, Chen S, Fu J, Zhao K, Chen G. Seismic performance of underground subway station with sliding between column and longitudinal beam. Tunn Undergr Space Technol 2020;102:103439. https://doi.org/10.1016/j.tust.2020.103439.
[34] Min Wang. Calculation and analysis on section control internal force for metro station structure. Modern Urban Transit 2013;3:72–5 [in Chinese)].
[35] Wang J-N. Seismic design of tunnels: a simple state-of-the-art design approach. Parsons Brinckerhoff; 1993. http://cdn.wspgroup.com/8kzmue/seismic-design-of-tunnels-a-simple-state-of-the-art-design-approach.pdf.
[36] Cilingir U, Madabhushi SPG. A model study on the effects of input motion on the seismic behavior of tunnels. Soil Dynam Earthq Eng 2011;31:452–62. https://doi.org/10.1016/j.soildyn.2010.10.004.
[37] Cilingir U, Madabhushi SPG. Effect of depth on the seismic response of square tunnels. Soils Found 2011;51(3):449–57. https://doi.org/10.3208/sandf.51.449.
[38] Tsinidis G, Pitilakis K, Madabhushi SPG, Heron C. Dynamic response of flexible square tunnels: centrifuge testing and validation of existing design methodologies. Geotechnique 2015;65(5):401–17. https://doi.org/10.1680/geot.SIP.15.P.004.
[39] Abuhajar O, El Naggar H, Newson T. Experimental and numerical investigations of the effect of buried box culverts on earthquake excitation. Soil Dynam Earthq Eng 2015;79:130–48. https://doi.org/10.1016/j.soildyn.2015.07.015.
[40] Tsinidis G, Pitilakis K, Madabhushi SPG. On the dynamic response of square tunnels in sand. Eng Struct 2016;125:419–37. https://doi.org/10.1016/j.engstruct.2016.07.014.
[41] Tsinidis G, Rovithis E, Pitilakis K, Chazelas JL. Seismic response of box-type tunnels in soft soil: experimental and numerical investigation. Tunn Undergr Space Technol 2016;59:199–214. https://doi.org/10.1016/j.tust.2016.07.008.
[42] Tsinidis G. Response characteristics of rectangular tunnels in soft soil subjected to transversal ground shaking. Tunn Undergr Space Technol 2017;62:1–22. https://doi.org/10.1016/j.tust.2016.11.003.
[43] Tsinidis G, Pitilakis K. Improved RF relations for the transversal seismic analysis of rectangular tunnels. Soil Dynam Earthq Eng 2018;107:48–65. https://doi.org/10.1016/j.soildyn.2018.01.004.
[44] Tsinidis G, de Silva F, Anastasopoulos I, Bilotta E, Bobet A, Hashash YM, He C, Kampas G, Knappett J, Madabhushi G, Nikitas N. Seismic behaviour of tunnels: from experiments to analysis. Tunn Undergr Space Technol 2020;99:103334. https://doi.org/10.1016/j.tust.2020.103334.
[45] Bardet JP, Ichii K, Lin CH. EERA: a computer program for equivalent-linear earthquake site response analyses of layered soil deposits. University of Southern California, Department of Civil Engineering; 2000. http://www.ce.memphis.edu/7137/PDFs/EERA2/EERAManual.pdf.
[46] Abaqus. 6.16 Documentation (Abaqus). Abaqus user's guide 2016. 2016.
[47] GB50909–2014 Code for seismic design of urban rail transit structures. Beijing, China: China Planning Press; 2014.
[48] Lysmer J, Kuhlemeyer RL. Finite dynamic model for infinite media. J Eng Mech Div 1969;95(4):859–77. https://doi.org/10.1061/JMCEA3.0001144.
[49] Deeks AJ, Randolph MF. Axisymmetric time-domain transmitting boundaries. J Eng Mech 1994;120(1):25–42. https://doi.org/10.1061/(ASCE)0733-9399(1994)120:1(25).

[50] Du X, Zhao M. A local time-domain transmitting boundary for simulating cylindrical elastic wave propagation in infinite media. Soil Dynam Earthq Eng 2010;30(10):937–46. https://doi.org/10.1016/j.soildyn.2010.04.004.
[51] Jingbo L, Shu L, Xiuli D. A method for the analysis of dynamic response of structure containing non-smooth contactable interfaces. Acta Mech Sinica-PRC 1999;15(1):63–72. https://doi.org/10.1007/BF02487902.
[52] Liu J, Du Y, Du X, Wang Z, Wu J. 3D viscous-spring artificial boundary in time domain. Earthq Eng Eng Vib 2006;5(1):93–102. https://doi.org/10.1007/s11803-006-0585-2.
[53] Patil M, Choudhury D, Ranjith PG, Zhao J. Behavior of shallow tunnel in soft soil under seismic conditions. Tunn Undergr Space Technol 2018;82:30–8. https://doi.org/10.1016/j.tust.2018.04.040.
[54] Jiang J, El Nggar HM, Xu C, Zhong Z, Du X. Effect of ground motion characteristics on seismic fragility of subway station. Soil Dynam Earthq Eng 2021;143:106618. https://doi.org/10.1016/j.soildyn.2021.106618.
[55] Kuhlemeyer RL, Lysmer J. Finite element method accuracy for wave propagation problems. J Soil Mech Found Div 1973;99(5):421–7. https://doi.org/10.1061/JSFEAQ.0001885.
[56] Lubliner J, Oliver J, Oller S, Oñate E. A plastic-damage model for concrete. Int J Solid Struct 1989;25(3):299–326. https://doi.org/10.1016/0020-7683(89)90050-4.
[57] Lee J, Fenves GL. Plastic-damage model for cyclic loading of concrete structures. J Eng Mech 1998;124(8):892–900. https://doi.org/10.1061/(ASCE)0733-9399(1998)124:8(892).
[58] GB50010–2010 Code for design of concrete structures. Beijing, China: China Architecture and Building Press; 2011.
[59] Hashash YMA, Park D. Viscous damping formulation and high frequency motion propagation in non-linear site response analysis. Soil Dynam Earthq Eng 2002;22(7):611–24. https://doi.org/10.1016/S0267-7261(02)00042-8.
[60] Yoshida N, Kobayashi S, Suetomi I, Miura K. Equivalent linear method considering frequency dependent characteristics of stiffness and damping. Soil Dynam Earthq Eng 2002;22(3):205–22. https://doi.org/10.1016/S0267-7261(02)00011-8.
[61] Xu Zi-gang, Xiu-li Du, Cheng-shun Xu, Zhang Chi-yu, Jia-wei Jiang. Comparative study of determination methods for Rayleigh damping coefficients of site in seismic responses analysis of underground structures. Rock Soil Mech 2019;40(12):4838–47. https://doi.org/10.16285/j.rsm.2018.1913.
[62] Xu C, Zhang Z, Li Y, Du X. Validation of a numerical model based on dynamic centrifuge tests and studies on the earthquake damage mechanism of underground frame structures. Tunn Undergr Space Technol 2020;104:103538. https://doi.org/10.1016/j.tust.2020.103538.
[63] Xu Z, Du X, Xu C, Hao H, Bi K, Jiang J. Numerical research on seismic response characteristics of shallow buried rectangular underground structure. Soil Dynam Earthq Eng 2019;116:242–52. https://doi.org/10.1016/j.soildyn.2018.10.030.
[64] BS 5975:2008 + A1 Code of practice for temporary works procedures and the permissible stress design of false work. 2011.
[65] Hua-qun C, Wei-qing L, Shu-guang W. Application study on elastic sliding bearings in isolated high-rise building. Earthq Resist Eng Retrofit 2007;3. https://doi.org/10.16226/j.issn.1002-8412.2007.03.010.
[66] Zhuang HY, Yang J, Chen S, Fu JS, Chen GX. Seismic performance of underground subway station structure considering connection modes and diaphragm wall. Soil Dynam Earthq Eng 2019;127:105842. https://doi.org/10.1016/j.soildyn.2019.105842.
[67] Wang Jianning, Ma Guowei, Zhuang Haiyang, Dou Yuanming, Fu Jisai. Influence of diaphragm wall on seismic responses of large unequal-span subway station in liquefiable soils. Tunn Undergr Space Technol 2019;91. https://doi.org/10.1016/j.tust.2019.05.018.
[68] PEER. NGA Strong Motion Database. http://peer.berkeley.edu/NGA.
[69] NIED K-NET, KiK-Net, National Research Institute for Earth Science and Disaster Resilience. https://doi.org/10.17598/NIED.0004.
[70] Ma C, Lu D, Gao H, Du X, Qi C. Seismic performance improvement of underground frame structures by changing connection type between sidewalls and slab. 2021 Soil Dynam Earthq Eng 2021;149:106851. https://doi.org/10.1016/j.soildyn.2021.106851.